

N O T I C E

THIS DOCUMENT HAS BEEN REPRODUCED FROM
MICROFICHE. ALTHOUGH IT IS RECOGNIZED THAT
CERTAIN PORTIONS ARE ILLEGIBLE, IT IS BEING RELEASED
IN THE INTEREST OF MAKING AVAILABLE AS MUCH
INFORMATION AS POSSIBLE

REMOTE SENSING OF SEA STATE BY LASER ALTIMETERS

by

B. Tsai
C. S. Gardner

RRL Publication No. 514

Technical Report
December 1981

Supported by
Contract No. NASA NSG-5049

NATIONAL AERONAUTICS & SPACE ADMINISTRATION
Goddard Space Flight Center
Greenbelt, Maryland 20771



RADIO RESEARCH LABORATORY
DEPARTMENT OF ELECTRICAL ENGINEERING
COLLEGE OF ENGINEERING
UNIVERSITY OF ILLINOIS
URBANA, ILLINOIS 61801

(NASA-CR-165049) REMOTE SENSING OF SEA STATE BY LASER ALTIMETERS (ILLINOIS UNIV.)
51 P HC A04/NF A01 CSCL 08C

N82-14789

Unclas
08528

G3/48

REMOTE SENSING OF SEA STATE BY LASER ALTIMETERS

by

**B. Tsai
C. S. Gardner**

RRL Publication No. 514

**Technical Report
December 1981**

**Supported by
Contract No. NASA NSG-5049**

**NATIONAL AERONAUTICS & SPACE ADMINISTRATION
Goddard Space Flight Center
Greenbelt, Maryland 20771**

**RADIO RESEARCH LABORATORY
DEPARTMENT OF ELECTRICAL ENGINEERING
COLLEGE OF ENGINEERING
UNIVERSITY OF ILLINOIS
URBANA, ILLINOIS 61801**

ABSTRACT

The reflection of short laser pulses from the ocean surface is analyzed based on the specular point theory of scattering. The expressions for the averaged received signal, shot noise and speckle induced noise are derived for a direct detection system. It is found that the reflected laser pulses have an average shape closely related to the probability density function associated with the surface profile. This result is applied to estimate the mean sea level and Significant Wave Height from the receiver output of the laser altimeter.

TABLE OF CONTENTS

	Page
1. INTRODUCTION.	1
2. RECEIVED SIGNAL	3
3. OCEAN SURFACE STATISTICS.	15
4. TEMPORAL MOMENTS OF THE RECEIVED SIGNAL	19
5. WAVEFORM OF THE RECEIVED SIGNAL	24
6. NON-NORMAL INCIDENCE.	37
7. CONCLUSIONS	41
REFERENCES.	42
CUMULATIVE LIST OF RADIO RESEARCH LABORATORY REPORTS PREPARED UNDER NASA GRANT NSG-5049	44
PAPERS PUBLISHED.	46

LIST OF FIGURES

Figure		Page
1.	Geometry of the laser altimeter and ocean surface for normal incidence.	4
2.	Geometry of the surface normal of the specular point.	9
3.	Mean received waveforms for laser altimeters with different beam divergence angles.	26
4.	Mean received waveforms of the laser altimeter for different wind speed and SWH.	27
5.	Mean received waveforms of the laser altimeter for different wind speed and SWH.	28
6.	Mean received waveforms of the laser altimeter for different wind speed and SWH.	29
7.	Mean received waveforms of the laser altimeter for different wind speed and SWH.	30
8.	Mean received waveform of the laser altimeter for different values of the skewness coefficient.	33
9.	Mean received waveforms of the laser altimeter for different values of the skewness coefficient.	34
10.	Mean received waveforms of the laser altimeter for values of the skewness coefficient.	35
11.	Geometry of the laser altimeter and ocean surface for non-normal incidence.	38

1. INTRODUCTION

In a previous paper by Gardner [1], the statistical characteristics of short laser pulses (pulse length less than 1 cm) that have been reflected from the ground were studied. In this report, we extend the previous results to the case where the reflections occur at the ocean surface instead of from a ground target.

At near vertical incidence, the reflection of laser radiation from the ocean is mainly accounted for by the scattering from specular points which are randomly distributed on the ocean surface. If the laser pulse length is short compared to the surface height variations, the reflected pulses from the ocean will have an average shape related to the height probability density of the specular points as well as the overall probability density of the height variations. Therefore, a short-pulse laser altimeter can be used in the determination of sea states as well as the mean sea level.

Short-pulse satellite altimeters in the microwave range have been used with good results in observing sea states [2], [3]. For radar altimeters, the transmitted pulse width is typically a few nanoseconds or longer, and the antenna beam width is usually on the order of degrees. For laser altimeters, the transmitted pulse width can be as short as tens of picoseconds, and the laser divergence angle can be as small as 10 μ rad. Because of these significant differences in the transmitter parameters, previous results on the radar altimeter have to be examined before they are applied to the laser altimeter.

In this report, we first derive the received signal in Chapter 2. In Chapter 3, ocean surface statistics are discussed. The temporal

moments of returned pulses are examined in Chapter 4. In Chapter 5, waveforms of the received signal are calculated using both Gaussian and non-Gaussian ocean surface statistics. It is shown that, with comparable parameters, our results for laser altimeters parallel those of radar altimeters. Finally, in Chapter 6, the effect of non-normal incidence is considered.

2. RECEIVED SIGNAL

The geometry of the laser altimeter and ocean surface is illustrated in Figure 1. The altitude of the altimeter measured from the mean sea level is z . The 2-D surface profile is described by $\xi(\underline{\rho})$, and its corresponding slope in the x - and y -directions is denoted by $\xi_x(\underline{\rho})$ and $\xi_y(\underline{\rho})$, respectively, where $\underline{\rho}$ is the horizontal position vector on the ocean surface and is measured from the center of the laser footprint. Initially, we assume that the laser pulse is incident normal to the mean surface level. In Chapter 6, the effects of non-normal incidence are discussed.

We first derive the mutual coherence function at the receiver plane. The complex amplitude of the pulsed laser beam at the transmitting telescope is

$$U_T(\underline{r}, t) = f(t) a_T(\underline{r}) e^{i\omega_0 t} \quad (1)$$

where

$f(t)$ = laser pulse amplitude

$a_T(\underline{r})$ = complex amplitude cross-section of the laser beam

ω_0 = laser frequency

$\underline{r} = (x, y)$ = transverse coordinate vector.

Using the Fresnel diffraction formula, the field incident on the ocean surface is

$$U_i(\underline{r}, z, t) = T_a^{1/2} f\left(t - \frac{2z}{c} - \frac{r^2}{2cz}\right) a_i(\underline{r}, z) \exp\left[i\left(\omega_0 t - k_0 z - \frac{k_0}{2z} r^2\right)\right] \quad (2)$$

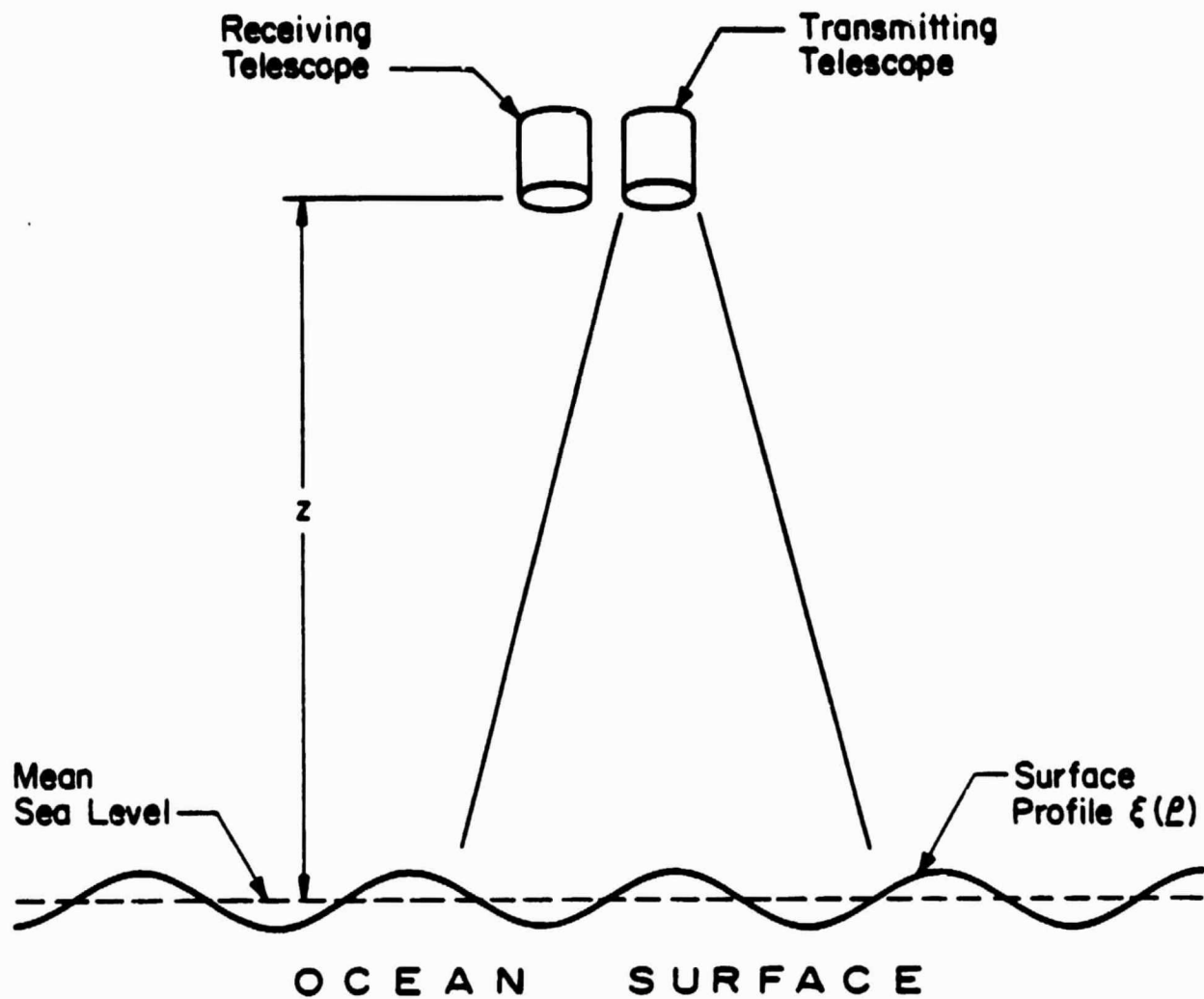


Figure 1. Geometry of the laser altimeter and ocean surface for normal incidence.

$$a_1(\underline{r}, z) = \frac{1}{\lambda_0 z} \int d^2 \rho a_T(\rho) \exp \left[-i \frac{k_0}{z} \left(\frac{\rho^2}{2} - \underline{r} \cdot \rho \right) \right] \quad (3)$$

T_a is the intensity transmittance of the atmosphere, k_0 is the wavenumber and λ_0 is the wavelength of the laser radiation. Throughout this paper, the spatial integrals are assumed to be evaluated over the entire plane. In deriving Equation (2), we have assumed that the rms laser pulse width (σ_f) and the area of the transmitting telescope (A_T) satisfy the condition

$$c\sigma_f \gg \frac{A_T}{z} \quad (4)$$

For near normal incidence, the reflection of laser light from the ocean surface is mainly accounted for by scattering from randomly distributed specular points on the surface. Since the ocean surface is very rough on the scale of the optical wavelength, the scattered power will be proportional to the number of specular points illuminated and the scattering cross-sections of specular points. According to the results of Kodis [4], each illuminated specular point scatters like the tangent sphere whose radius is the geometric mean of the two principal radii of the surface at the specular point. In the optical region, the scattering cross section of a sphere with radius R is just πR^2 [5]. Then, the reflected field in the plane immediately above the ocean surface is given by

$$U_s(\underline{r}, z, t) = R(0) [\pi n |r_a r_b|]^{1/2} H_1 \left(\underline{r}, z, t + \frac{2\xi(\underline{r})}{c} \right) \quad (5)$$

where

$R(0)$ = Fresnel reflection coefficient for normal incidence

$\xi(\underline{r})$ = surface elevation at \underline{r}

$|r_a r_b|$ = absolute value of product of principal radii of curvature
at the specular point

n = number density of specular points at the point of reflection.

$|r_a r_b|$ can be expressed in terms of the derivatives of the surface profile $\xi(\underline{r})$ as follows [6]

$$|r_a r_b| = \frac{(1 + \xi_x^2 + \xi_y^2)^2}{|\xi_{xx} \xi_{yy} - \xi_{xy}^2|} \quad (6)$$

where

$$\xi_{xx} = \frac{\partial^2 \xi}{\partial x^2}$$

$$\xi_{yy} = \frac{\partial^2 \xi}{\partial y^2}$$

$$\xi_{xy} = \frac{\partial^2 \xi}{\partial x \partial y}$$

Equation (5) implies that when the incident field is reflected it is reduced in amplitude and undergoes a propagation delay which is proportional to the surface height distribution. Therefore, the field in the plane of the receiving telescope is

$$U(\underline{r}, z, t) = a(\underline{r}, z, t) e^{i\omega_0 t} = \frac{T_a}{\lambda_0 z} \exp \left[i \left(\omega_0 t - 2k_0 z - \frac{k_0}{2z} r^2 \right) \right] \\ \cdot \int d^2 \rho a_1(\rho, z) R(0) [\pi n |r_a r_b|]^k f \left(t - \frac{2z}{c} - \frac{\rho^2}{cz} + \frac{2\xi(\rho)}{c} \right) \\ \cdot \exp \left\{ -ik_0 \left(\frac{\rho^2}{2z} - 2\xi(\rho) - \frac{\rho \cdot \underline{r}}{z} \right) \right\} \quad (7)$$

In deriving Equation (7), the laser pulse width and receiver aperture area A_R are assumed to satisfy the condition

$$c\sigma_f \gg \frac{A_R}{z} \quad (8)$$

The mutual coherence function is defined as

$$J_a(\underline{r}_1, t_1; \underline{r}_2, t_2) = \langle a(\underline{r}_1, z, t_1) a^*(\underline{r}_2, z, t_2) \rangle \quad (9)$$

where the angle bracket denotes expectation with respect to speckle and the microstructure of the surface.

Under the assumption that the ocean surface is rough on the scale of the optical wavelength and that the microstructure is unresolvable by the receiving telescope, we can first perform the expectation over speckle, and Equation (9) becomes

$$J_a(\underline{r}_1, t_1; \underline{r}_2, t_2) = T_a^2 z^{-2} |R(0)|^2 \pi \exp\left[-i \frac{k_0}{2z} (r_1^2 - r_2^2)\right] \int d^2 \rho |a_1(\rho, z)|^2 \langle n(\rho, \xi) \frac{(1 + \xi_x^2 + \xi_y^2)^2}{|\xi_{xx} \xi_{yy} - \xi_{xy}^2|} \rangle f(t_1 - \psi) f^*(t_2 - \psi) \exp\left[\frac{k_0}{z} \rho \cdot (\underline{r}_1 - \underline{r}_2)\right] \quad (10)$$

where

$$\psi = \frac{2z}{c} + \frac{\rho^2}{cz} - \frac{2\xi(\rho)}{c} \quad (11)$$

The expectation inside the integral in Equation (10) is with respect to the number of scatterers and their scattering cross-sections. By using the results of Barrick [6] and taking into account the ξ dependence, we have

$$\langle n(\rho, \xi) \frac{(1 + \xi_x^2 + \xi_y^2)^2}{|\xi_{xx} \xi_{yy} - \xi_{xy}^2|} \rangle = \pi (1 + \xi_x^2 + \xi_y^2)^2 p(\xi_x, \xi_y | \xi(\rho)) \quad (12)$$

where $p(\xi_x, \xi_y | \xi)$ is the joint probability density function of ξ_x and ξ_y at a given elevation ξ .

Since the ocean surface can be described by the equation

$$f(x, y, z) = z - \xi(x, y) = 0 \quad (13)$$

the surface normal at the specular point is obtained by taking the gradient of the left side of Equation (13)

$$\vec{n} = \nabla f = \hat{z} - \hat{x}\xi_x - \hat{y}\xi_y \quad (14)$$

where \hat{x} , \hat{y} , \hat{z} are unit vectors in the x-, y- and z-directions, and \vec{n} is the normal vector at the specular point. If we denote the angle between the z-axis and local surface normal \vec{n} as θ , then from Eq. (14) and Figure 2 we find that θ is related to the surface slopes at the specular point by

$$\tan \theta = (\xi_x^2 + \xi_y^2)^{1/2} \quad (15)$$

For backscatter, θ is also the incidence angle for the specular point. Equation (15) implies that only those specular points which are tilted so as to be normal to the incident wave are effective in contributing to the received field. This is not an unexpected result. Since θ is also the incidence angle, it can be related to the horizontal position of the specular point ρ by

$$\tan \theta = \frac{\rho}{z} \quad (16)$$

Note that we are assuming that ρ is measured from the center of the laser footprint. By substituting Equations (12), (15) and (16) into Equation (10), we obtain

$$\begin{aligned} J_a(\underline{r}_1, t_1; \underline{r}_2, t_2) &= T_a^2 z^{-2} \exp\left[-1 \frac{k_0}{2z} (r_1^2 - r_2^2)\right] |R(0)|^2 \pi \int d^2 \rho \\ &\cdot |a_1(\rho, z)|^2 \left[1 + \frac{\rho^2}{z^2}\right]^2 P(\xi_x, \xi_y | \xi(\psi)) f(t_1 - \psi) f^*(t_2 - \psi) \\ &\cdot \exp\left[1 \frac{k_0}{z} \rho \cdot (\underline{r}_1 - \underline{r}_2)\right] \end{aligned} \quad (17)$$

We assume that the receiver field-of-view and interference filter are adjusted so that all the signal energy which is incident on the telescope

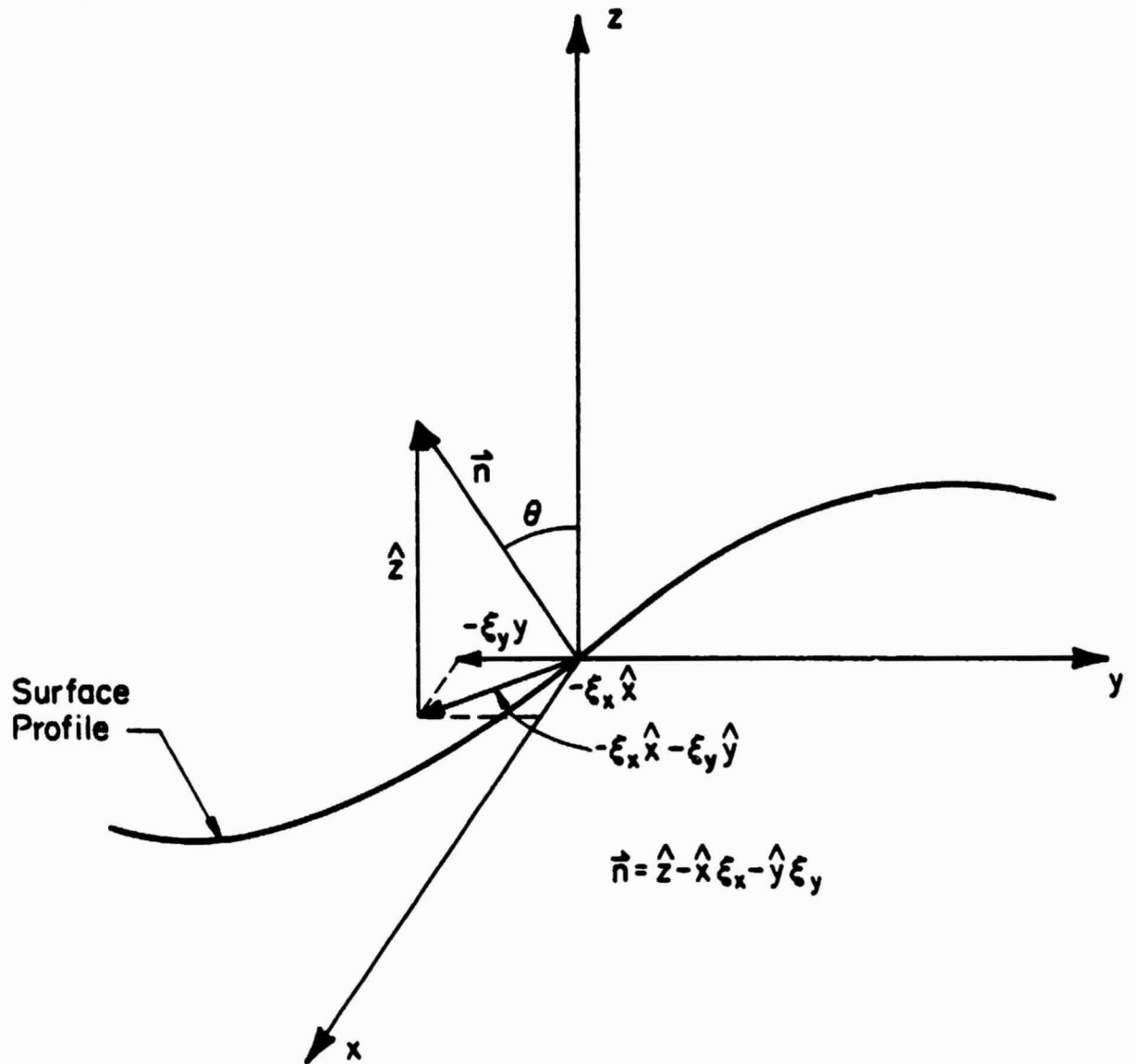


Figure 2. Geometry of the surface normal of the specular point.

objective is focussed onto the photodetector. Therefore, the total received signal power is given by

$$P(t) = \int d^2\underline{r} W(\underline{r}) |a(\underline{r}, z, t)|^2 \quad (18)$$

where $W(\underline{r})$ is an appropriate aperture weighting function. $W(\underline{r})$ is equal to one for \underline{r} inside the aperture and zero otherwise. For direct detection, the mean and covariance of the signal at the receiver output can be calculated using Campbell's theorem [7]

$$\begin{aligned} E[s(t)] &= \frac{\eta}{hf_0} E[P(t)] * h(t) \quad (19) \\ C_s(t_1, t_2) &= \frac{\eta}{hf_0} \int_{-a}^{\infty} d\tau E[P(\tau)] h(t_1 - \tau) h(t_2 - \tau) \\ &\quad + \left[\frac{\eta}{hf_0} \right]^2 \int_{-\infty}^{\infty} d\tau_1 \int_{-\infty}^{\infty} d\tau_2 C_p(\tau_1, \tau_2) h(t_1 - \tau_1) h(t_2 - \tau_2) \quad (20) \end{aligned}$$

η is the efficiency of the receiver optics and detector, hf_0 is the energy of one signal photon, $h(t)$ is the impulse response of the receiver electronics, and C_p is the temporal covariance of the received signal power.

The variance of $s(t)$ may be regarded as the signal induced noise. The first term in Equation (20) is the quantum or shot noise component of the covariance. The second term arises from the randomness of the scattering cross-section, surface profile, and the speckle induced fluctuation.

Since the amplitude of the received field for a given realization of the surface profile is a circular complex Gaussian process, the expected value and covariance of $P(t)$ can be written in terms of the mutual coherence function of the received optical field.

$$E[P(t) | \xi] = \int d^2\underline{r} J_a(\underline{r}, t; \underline{r}, t) W(\underline{r}) \quad (21)$$

The unconditioned mean received power is obtained by taking the expectation with respect to surface profile.

$$\begin{aligned}
 E\{P(t)\} &= E\{E\{P(t)|\xi\}\} \\
 &= A_R T_a^2 z^{-2} |R(0)|^2 \pi \int d^2 \underline{\rho} |a_1(\underline{\rho}, z)|^2 \left(1 + \frac{\rho^2}{z^2}\right)^2 \int d\xi p(\xi_x, \xi_y, \xi) \\
 &\quad \cdot |f(t - \psi)|^2
 \end{aligned} \tag{22}$$

where $p(\xi_x, \xi_y, \xi)$ is the joint probability density of ξ_x , ξ_y and ξ .

By substituting Equation (22) into Equation (19), the mean waveform at the receiver output can be expressed as

$$\begin{aligned}
 E\{s(t)\} &= \frac{\eta}{h f_0} A_R T_a^2 z^{-2} |R(0)|^2 \pi \int d^2 \underline{\rho} |a_1(\underline{\rho}, z)|^2 \left(1 + \frac{\rho^2}{z^2}\right)^2 \\
 &\quad \cdot \int d\xi p(\xi_x, \xi_y, \xi) g\left(t - \frac{2z}{c} - \frac{\rho^2}{cz} + \frac{2\xi(\underline{\rho})}{c}\right)
 \end{aligned} \tag{23}$$

where $g(t) = |f(t)|^2 * h(t)$ is the point target response of the laser altimeter. In Equation (23), the integration over ξ is recognized to be the convolution of altimeter point target response g with the joint probability density function $p(\xi_x, \xi_y, \xi)$.

The power covariancefunction of the received field is defined as

$$C_p(t_1, t_2) = E\{P(t_1) P(t_2)\} - E\{P(t_1)\} E\{P(t_2)\} \tag{24}$$

The first term in Equation (24) can be written in terms of the amplitude of the received field as

$$\begin{aligned}
 &E\{P(t_1) P(t_2)\} \\
 &= \int d^2 \underline{r}_1 \int d^2 \underline{r}_2 E\{<a(\underline{r}_1, t_1) a^*(\underline{r}_1, t_1) a(\underline{r}_2, t_2) a^*(\underline{r}_2, t_2)>\} W(\underline{r}_1) W(\underline{r}_2)
 \end{aligned} \tag{25}$$

where the inner angle bracket is the expectation with respect to the speckle and microstructure of the surface, and the outside expectation is with respect to the surface profile ξ .

Using the properties of the circular complex Gaussian fields [8], the expectation over speckle and microstructure is carried out and expressed in terms of mutual coherence function

$$E\{P(t_1) P(t_2)\} = \int d^2\underline{r}_1 \int d^2\underline{r}_2 W(\underline{r}_1) W(\underline{r}_2) E[J_a(\underline{r}_1, t_1; \underline{r}_1, t_1) J_a(\underline{r}_2, t_2; \underline{r}_2, t_2) + |J_a(\underline{r}_1, t_1; \underline{r}_2, t_2)|^2] \quad (26)$$

The expectation inside the integral is over the surface profile, which can be written explicitly in terms of the probability distribution functions of the surface profile. The first term in Equation (26) becomes

$$\begin{aligned} & \int d^2\underline{r}_1 \int d^2\underline{r}_2 W(\underline{r}_1) W(\underline{r}_2) E[J_a(\underline{r}_1, t_1; \underline{r}_1, t_1) J_a(\underline{r}_2, t_2; \underline{r}_2, t_2)] \\ &= T_a^4 z^{-4} |R(0)|^4 \pi^2 A_R^2 \int d^2\underline{\rho}_1 \int d^2\underline{\rho}_2 |a_1(\underline{\rho}_1, z)|^2 |a_1(\underline{\rho}_2, z)|^2 \left(1 + \frac{\rho_1^2}{z^2}\right)^2 \left(1 + \frac{\rho_2^2}{z^2}\right)^2 \\ & \cdot \int d\xi_1 \int d\xi_2 p(\xi_{x_1}, \xi_{y_1} | \xi_1) p(\xi_{x_2}, \xi_{y_2} | \xi_2) p(\xi_1(\underline{\rho}_1), \xi_2(\underline{\rho}_2)) \\ & \cdot |f(t_1 - \psi_1)|^2 |f(t_2 - \psi_2)|^2 \end{aligned} \quad (27)$$

where $p(\xi_1(\underline{\rho}_1), \xi_2(\underline{\rho}_2))$ is the joint probability density of surface heights at $\underline{\rho}_1$ and $\underline{\rho}_2$.

The second term in Equation (26) can be simplified by noting that the mutual intensity function only depends on the difference coordinate $(\underline{r}_1 - \underline{r}_2)$. By making the change of variables $\underline{r} = \underline{r}_1 - \underline{r}_2$ and $\underline{r}_g = \frac{\underline{r}_1 + \underline{r}_2}{2}$ in Equation (26), the integration over \underline{r}_g can be carried out to give

$$\int d^2\underline{x}_1 \int d^2\underline{x}_2 W(\underline{x}_1) W(\underline{x}_2) \mathbb{E}[|J_a(\underline{x}_1, t_1; \underline{x}_2, t_2)|^2]$$

$$= \int d^2\underline{x} R_W(\underline{x}) \mathbb{E}[|J_a(\underline{x}/2, t_1; -\underline{x}/2, t_2)|^2] \quad (28)$$

where R_W is the autocorrelation function of the receiver aperture

$$R_W(\underline{x}) = \int d^2\underline{\rho} W(\underline{\rho}) W(\underline{\rho} + \underline{x}) \quad (29)$$

Notice that the maximum value of R_W occurs when $\underline{x} = 0$ and is equal to the aperture area. Normally, the diameter of the receiver aperture will be large compared to the speckle correlation length [9]. In this case, $R_W(\underline{x})$ will be approximately constant over the important area of integration so that Equation (28) can be approximated by

$$\int d^2\underline{x} R_W(0) \mathbb{E}[|J_a(\underline{x}/2, t_1; -\underline{x}/2, t_2)|^2]$$

$$= R_W(0) \int d^2\underline{x} \mathbb{E}[|J_a(\underline{x}/2, t_1; -\underline{x}/2, t_2)|^2] \quad (30)$$

The integration over \underline{x} in Equation (30) can be easily evaluated. By taking the expectation over ξ , we have

$$R_W(0) \int d^2\underline{x} \mathbb{E}[|J_a(\underline{x}/2, t_1; -\underline{x}/2, t_2)|^2]$$

$$= \lambda_{0T}^2 \lambda_a^4 z^{-2} |R(0)|^4 \pi^2 A_R \int d^2\underline{\rho} |a_1(\underline{\rho}, z)|^4 \left(1 + \frac{\rho^2}{z^2}\right)^4 \int d\xi p^2(\xi_x, \xi_y | \xi) p(\xi)$$

$$\cdot |f(t_1 - \psi)|^2 |f(t_2 - \psi)|^2 \quad (31)$$

Finally, the power covariance function of the received field can be obtained by substituting Equations (22), (27) and (31) into Equation (24)

$$\begin{aligned}
C_p(t_1, t_2) = & \lambda_o^2 T_a^4 z^{-2} |R(0)|^4 \pi^2 A_R \int d^2 \rho |a_1(\rho, z)|^4 \left(1 + \frac{\rho^2}{z^2}\right)^4 \\
& \cdot \int d\xi p^2(\xi_x, \xi_y | \xi) p(\xi) |f(t_1 - \psi)|^2 |f(t_2 - \psi)|^2 \\
& + T_a^4 z^{-4} |R(0)|^4 \pi^2 A_R^2 \int d^2 \rho_1 \int d^2 \rho_2 |a_1(\rho_1, z)|^2 |a_1(\rho_2, z)|^2 \\
& \cdot \left(1 + \frac{\rho_1^2}{z^2}\right)^2 \left(1 + \frac{\rho_2^2}{z^2}\right)^2 \int d\xi_1 \int d\xi_2 |f(t_1 - \psi_1)|^2 |f(t_2 - \psi_2)|^2 \\
& \cdot [p(\xi_{x_1}, \xi_{y_1} | \xi_1) p(\xi_{x_2}, \xi_{y_2} | \xi_2) p(\xi_1, \xi_2) - p(\xi_{x_1}, \xi_{y_1}, \xi_1) p(\xi_{x_2}, \xi_{y_2}, \xi_2)] \\
& \hspace{15em} (32)
\end{aligned}$$

The covariance of the output signal is obtained by substituting Equations (22) and (32) into Equation (20)

$$\begin{aligned}
C_s(t_1, t_2) = & \left[\frac{\eta}{hf_o}\right] T_a^2 z^{-2} |R(0)|^2 \pi A_R \int d^2 \rho |a_1(\rho, z)|^2 \left(1 + \frac{\rho^2}{z^2}\right)^2 \\
& \cdot \int d\xi p(\xi_x, \xi_y, \xi) \int_{-\infty}^{\infty} d\tau |f(\tau - \psi)|^2 h(t_1 - \tau) h(t_2 - \tau) \\
& + \left[\frac{\eta}{hf_o}\right]^2 \lambda_o^2 T_a^4 z^{-2} |R(0)|^4 \pi^2 A_R \int d^2 \rho |a_1(\rho, z)|^4 \left(1 + \frac{\rho^2}{z^2}\right)^4 \int d\xi \\
& \cdot p^2(\xi_x, \xi_y | \xi) p(\xi) g(t_1 - \psi) g(t_2 - \psi) \\
& + \left[\frac{\eta}{hf_o}\right]^2 T_a^4 z^{-4} |R(0)|^4 \pi^2 A_R \int d^2 \rho_1 \int d^2 \rho_2 |a_1(\rho_1, z)|^2 |a_1(\rho_2, z)|^2 \\
& \cdot \left(1 + \frac{\rho_1^2}{z^2}\right)^2 \left(1 + \frac{\rho_2^2}{z^2}\right)^2 \int d\xi_1 \int d\xi_2 g(t_1 - \psi_1) g(t_2 - \psi_2) \\
& \cdot [p(\xi_{x_1}, \xi_{y_1} | \xi_1) p(\xi_{x_2}, \xi_{y_2} | \xi_2) p(\xi_1, \xi_2) - p(\xi_{x_1}, \xi_{y_1}, \xi_1) \\
& p(\xi_{x_2}, \xi_{y_2}, \xi_2)] \\
& \hspace{15em} (33)
\end{aligned}$$

3. OCEAN SURFACE STATISTICS

The wave height at any given point on the ocean surface is the resultant of many wave components that have been generated by the wind in different regions and have propagated to the point of observation. Since the interactions between each wave component are weak [10], their motions are assumed to be weakly correlated. Therefore, under the central-limit theorem, we expect the distribution of wave height to approach a Gaussian.

The first approximation to the distribution of wave height is then

$$p(\xi) = (2\pi\sigma_{\xi}^2)^{-1/2} \exp\left(-\frac{\xi^2}{2\sigma_{\xi}^2}\right) \quad (34)$$

where σ_{ξ} is the rms wave height.

Significant Wave Height, SWH, is defined as the average of heights (from crest to trough) of the one-third-highest waves observed at a point. It is approximately equal to 4 times the rms wave height of the ocean surface [3].

$$SWH = 4 \sigma_{\xi} \quad (35)$$

The rms wave height can be related to the wind speed by integrating the Phillips' wind-wave-height spectrum [11]

$$\sigma_{\xi} = 0.016 W^2 \text{ meter} \quad (36)$$

where W is the averaged wind speed in meters per second measured at 12.5 meters above the sea level.

The first approximation to the joint distribution of the wave slopes is also Gaussian [12]

$$p(\xi_x, \xi_y) = \frac{1}{\pi S^2} \exp\left(-\frac{\xi_x^2 + \xi_y^2}{S^2}\right) \quad (37)$$

where S^2 is the mean square value of the total slope, defined as

$$S^2 = \langle \xi_x^2 \rangle + \langle \xi_y^2 \rangle \quad (38)$$

An empirical relationship between S^2 and wind speed is given by Cox and Munk [13] as

$$S^2 = 0.003 + 0.00512 W \quad (39)$$

where W is in meters per second and S is dimensionless. However, the actual surface profile cannot be an exact Gaussian for two reasons. First, the wave height can never go to infinity. Second, due to the presence of weak nonlinear interactions between wave components, the actual ocean surface is not symmetric about the mean, as predicted by a Gaussian distribution. This is born out by the observation that, on the ocean surface, wave crests tend to be relatively high and sharp, while the wave troughs are comparatively smooth and shallow. Mathematically, this fact could be taken into account by including higher-order terms containing skewness and kurtosis in the probability density functions given by Equations (34) and (37).

It is simple to show that surface elevation and surface slopes are uncorrelated at the same point. Therefore, if a Gaussian surface profile is assumed, the surface elevation and slope are independent. Thus, the joint density function of surface height and slopes can be factored as

$$p(\xi, \xi_x, \xi_y) = p(\xi_x, \xi_y) p(\xi) \quad (40)$$

One important implication of Equation (40) is that the scattering cross-section will be the same from wave crest to wave trough, independent of ξ . But, the experimental results obtained by Yaplee et al. [14] for a 1 GHz, 1-ns pulsed radar indicated an approximately linear increase of scattering cross-section from wave crest to wave trough. On the other hand, experimental results obtained in the optical range, using N_2 , YAG and CO_2 lasers, indicate that maximum reflection may occur at the wave crest [15]. Therefore, the mean sea level "seen" by the altimeter would be different from the true sea level.

Jackson [16] derived the expression for the joint probability density function of wave height and slope, which takes into account the non-Gaussian behavior of the sea waves. His result is the following

$$p(\xi_x, \xi) = [2\pi(\sigma_\xi^2 \langle \xi_x^2 \rangle)^{1/2}]^{-1} \exp \left[-\frac{1}{2} \left[\frac{\xi^2}{\sigma_\xi^2} + \frac{\xi_x^2}{\langle \xi_x^2 \rangle} \right] \right] \\ \cdot \left[1 + \frac{\lambda_3}{6} \left[\frac{\xi^3}{\sigma_\xi^3} - 9 \frac{\xi}{\sigma_\xi} + 6 \frac{\xi}{\sigma_\xi} \frac{\xi_x^2}{\langle \xi_x^2 \rangle} \right] \right] \quad (41)$$

where λ_3 is the skewness coefficient which is defined by

$$\lambda_3 = \frac{\langle \xi^3 \rangle}{\sigma_\xi^3} \quad (42)$$

In arriving at Equation (41), Jackson assumed a long crested or corrugated sea surface and made use of the one-dimensional Phillips' saturated wave number spectrum. However, Equation (41) does not include the effect of capillary waves, whose statistics are still uncertain.

Capillary waves are waves with wavelengths less than approximately 1.7 cm. They will not be seen by a radar altimeter with wavelengths of 10 cm or larger, but will be seen by the laser altimeter. Therefore, the validity of Equation (41) in the optical range remains questionable. In the absence of a more accurate expression, we make use of Equation (39) in some derivations, keeping in mind that the actual skewness terms could be different in both magnitude and sign.

For vertical incidence, we need the expression for $p(\xi_x, \xi_y, \xi)$ evaluated at $\xi_x = \xi_y = 0$. Although the expression for $p(\xi_x, \xi)$ alone is not enough for us to obtain the general expression for $p(\xi_x, \xi_y, \xi)$, it does allow us to obtain the desired expression for $p(0, 0, \xi)$. By substituting S^2 for $\langle \xi_x^2 \rangle$ in Equation (41), and evaluating at $\xi_x = 0$, we have

$$p(0, 0, \xi) = [(2\pi^3)^{1/2} S^2 \sigma_\xi^2]^{-1/2} \exp \left[-\frac{1}{2} \frac{\xi^2}{\sigma_\xi^2} \right] \left[1 + \frac{\lambda_3}{6} \left[\frac{\xi^3}{\sigma_\xi^3} - 9 \frac{\xi}{\sigma_\xi} \right] \right] \quad (43)$$

Equation (43) is very similar to the marginal distribution of wave height with the skewness term included

$$p(\xi) = (2\pi\sigma_\xi^2)^{-1/2} \exp \left[-\frac{\xi^2}{2\sigma_\xi^2} \right] \left[1 + \frac{\lambda_3}{6} \left[\frac{\xi^3}{\sigma_\xi^3} - 3 \frac{\xi}{\sigma_\xi} \right] \right] \quad (44)$$

It will be shown that, if Equation (43) is used in Equation (23) for the returned signal, the mean sea level seen by the altimeter is biased by the amount $\lambda_3 \sigma_\xi$. With the inherent high accuracy of laser altimeters, this bias is significant, and should be considered in the processing of received signals.

4. TEMPORAL MOMENTS OF THE RECEIVED SIGNAL

In this chapter, temporal moments of the received signal are derived. For simplicity, we assume the surface profile is Gaussian, so that we can use Equation (40) to factor the joint density of surface slopes and elevation.

The temporal moments of the received signal are related to the statistics of the ocean surface profile. The k^{th} -order moment is defined as

$$m_k = \int_{-\infty}^{\infty} dt t^k S(t) \quad (45)$$

The zeroth-order moment, m_0 , is proportional to the total received signal energy. The expected value of m_0 is calculated using Equations (23) and (40)

$$\langle m_0 \rangle = \langle N \rangle G \quad (46)$$

where

$$\langle N \rangle = \frac{\eta}{hf_0} \beta_r Q T_{aR}^2 z^{-2} \quad (47)$$

$$G = \int_{-\infty}^{\infty} dt h(t) \quad (48)$$

$$Q = \int d^2 \rho |a_1(\rho, z)|^2 \int_{-\infty}^{\infty} dt |f(t)|^2 \quad (49)$$

$$\beta_r = Q^{-1} |R(0)|^2 \pi \int d^2 \rho |a_1(\rho, z)|^2 \left(1 + \frac{\rho^2}{z^2} \right)^2 P(\xi_x, \xi_y) \int_{-\infty}^{\infty} dt |f(t)|^2 \quad (50)$$

$\langle N \rangle$ is the expected number of detected signal photons per received pulse, G is the gain of the receiver electronics, Q is the total energy transmitted

per laser pulse, and β_r is the equivalent power reflection coefficient of the entire laser footprint. Generally, β_r is a function of the sea state within the laser footprint.

To compute the statistics of the temporal moments, it is convenient to express the mean and covariance of the receiver output in terms of $\langle n_0 \rangle$. From Equations (23), (33) and (46), we obtain

$$E[s(t)] = \langle N \rangle \int d^2 \rho b_2(\rho, z) \int d\xi P(\xi) g(t - \psi) \quad (51)$$

$$\begin{aligned} C_s(t_1, t_2) = & \langle N \rangle \int d^2 \rho b_2(\rho, z) \int d\xi P(\xi) \int_{-\infty}^{\infty} d\tau |\xi(t - \psi)|^2 h(t_1 - \tau) h(t_2 - \tau) \\ & + \langle N \rangle^2 k_s^{-1} \int d^2 \rho b_4(\rho, z) \int d\xi P(\xi) g(t_1 - \psi) g(t_2 - \psi) \\ & + \langle N \rangle^2 \int d^2 \rho_1 \int d^2 \rho_2 b_2(\rho_1, z) b_2(\rho_2, z) \int d\xi_1 \int d\xi_2 [P(\xi_1, \xi_2) \\ & - P(\xi_1) P(\xi_2)] g(t_1 - \psi_1) g(t_2 - \psi_2) \end{aligned} \quad (52)$$

where

$$\begin{aligned} b_n(\rho, z) = & |a_1(\rho, z)|^n \left(1 + \frac{\rho^2}{z^2} \right)^n p^{n/2}(\xi_x, \xi_y) / \int d^2 \rho |a_1(\rho, z)|^n \\ & \cdot \left(1 + \frac{\rho^2}{z^2} \right)^n p^{n/2}(\xi_x, \xi_y) \end{aligned} \quad (53)$$

$$\begin{aligned} K_s = & A_R(\lambda_0 z)^{-2} \left[\int d^2 \rho |a_1(\rho, z)|^2 \left(1 + \frac{\rho^2}{z^2} \right)^2 p(\xi_x, \xi_y) \right]^2 \\ & \cdot \left[\int d^2 \rho |a_1(\rho, z)|^4 \left(1 + \frac{\rho^2}{z^2} \right)^4 p^2(\xi_x, \xi_y) \right]^{-1} \end{aligned} \quad (54)$$

For $n = 2$, $b_2(\rho, z)$ is the normalized effective cross-section of the laser beam. K_s is the ratio of the receiver aperture area to the speckle correlation area. The speckle correlation area is inversely proportional to the area of the laser footprint. Typically, K_s is much greater than one [9].

We are primarily interested in the normalized moments

$$\frac{m_k}{m_0} = \int_{-\infty}^{\infty} dt t^k S(t) / \int_{-\infty}^{\infty} dt S(t) \quad (55)$$

If we assume the fluctuations in $S(t)$ due to shot noise and speckle are small, the mean of m_k/m_0 can be written as [1]

$$E \left[\frac{m_k}{m_0} \right] = \frac{\langle m_k \rangle}{\langle m_0 \rangle} \quad (56)$$

where

$$\langle m_k \rangle = \int_{-\infty}^{\infty} dt t^k E[S(t)] \quad (57)$$

The variance of m_0 is

$$\text{Var}(m_0) = \int_{-\infty}^{\infty} dt_1 \int_{-\infty}^{\infty} dt_2 C_s(t_1, t_2) \quad (58)$$

By substituting Equation (52) into Equation (58) and carrying out the integrations, we obtain

$$\text{Var}(m_0) = \langle N \rangle G^2 + \langle N \rangle^2 G^2 K_s^{-1} \quad (59)$$

The first-order normalized moment is the time delay between the firing of the laser pulse and the centroid of the received pulse. This delay

can be used to estimate the altitude of the altimeter above the sea level. If we denote the received signal time delay by T_s , then the expected delay can be written as

$$\langle T_s \rangle = E \left[\frac{a_1}{a_0} \right] \quad (60)$$

By using Equation (54), Equation (58) can be evaluated to give

$$\langle T_s \rangle = \int d^2 \underline{\rho} b_2(\underline{\rho}, z) \int d\xi p(\xi) \psi \quad (61)$$

Using the expression in Equation (9) for ψ , Equation (59) can be simplified

$$\langle T_s \rangle = \frac{2z}{c} + \frac{\sigma_r^2}{cz} + \frac{2\langle \xi \rangle}{c} \quad (62)$$

where

$$\sigma_r^2 = \int d^2 \underline{\rho} \rho^2 b_2(\underline{\rho}, z) \quad (63)$$

For Gaussian surface profile, $\langle \xi \rangle = 0$. It will be shown later that if the non-Gaussian nature of the surface profile is taken into account, a term proportional to the skewness coefficient is added to the right side of Equation (62). The expected delay given in Equation (62) is composed of two terms. z is the altitude of the altimeter measured from mean sea level. Therefore, $\frac{2z}{c}$ represents the round-trip propagation delay along a line normal to the surface. σ_r is the rms width of the effective laser footprint seen by the receiver aperture. The term $\frac{\sigma_r^2}{cz}$ represents the additional propagation delay resulting from the curvature of the diverging laser beam.

The mean-square width of the received pulse is

$$\sigma_s^2 = \frac{\int_{-\infty}^{\infty} dt (t - T_s)^2 S(t)}{\int_{-\infty}^{\infty} dt S(t)} \quad (64)$$

The expected value of the pulse width can be calculated to give

$$E[\sigma_s^2] = \sigma_h^2 + \sigma_f^2 + \frac{4}{c^2} \sigma_\xi^2 + (cz)^{-2} \int d^2\rho (\rho^2 - \sigma_r^2)^2 b_2(\rho, z) \quad (65)$$

where σ_h^2 is the mean-square width of $h(t)$, σ_f^2 is the mean-square width of the transmitted laser pulse ($|f|^2$), and σ_ξ^2 is the variance of the ocean surface profile. σ_h^2 and σ_f^2 in Equation (65) can be computed from the known parameters of the altimeter. Both the third term and the last term depend on the sea states within the footprint. Therefore, the width of the received pulse can be used to obtain information about ocean surface conditions. This is discussed in detail in the next chapter.

5. WAVEFORM OF THE RECEIVED SIGNAL

The laser cross-section and waveform of the transmitted laser pulse are assumed to be Gaussian in shape

$$|a_1(\rho, z)|^2 = E_0 [2\pi\sigma_1^2(z)]^{-1} \exp\left[-\frac{\rho^2}{2\sigma_1^2(z)}\right] \quad (66)$$

$$|f(t)|^2 = (2\pi\sigma_f^2)^{-1/2} \exp\left[-\frac{t^2}{2\sigma_f^2}\right] \quad (67)$$

where E_0 is the total energy of the transmitted laser pulse, and $\sigma_1(z)$ is the rms width of the transmitting laser cross section. $\sigma_1(z)$ is related to the divergence angle of the transmitted laser beam θ_T and the altitude of the altimeter z by

$$\sigma_1 = z \tan \theta_T \quad (68)$$

In addition, the response of the receiver is assumed to be given by

$$h(t) = G(2\pi\sigma_h^2)^{-1/2} \exp\left[-\frac{t^2}{2\sigma_h^2}\right] \quad (69)$$

where G is the gain of the receiver.

The point target or impulse response of the altimeter, defined previously as $g(t) = |f(t)|^2 * h(t)$, can be expressed explicitly by using Equations (65) and (67)

$$g(t) = G(2\pi\sigma_g^2)^{-1/2} \exp\left[-\frac{t^2}{2\sigma_g^2}\right] \quad (70)$$

where

$$\sigma_g^2 = \sigma_h^2 + \sigma_f^2 \quad (71)$$

If Gaussian surface statistics are assumed, we can substitute Equations (34), (37), (66) and (70) into Equation (23) and carry out the integration. The result is

$$E[(S(t))] = \langle N \rangle \frac{c\bar{x}}{4\pi\sigma_r^2} \exp\left[\frac{\sigma_c^2 z^2}{8\sigma_r^2} - \frac{c\bar{x}}{2\sigma_r^2} \left(t - \frac{2z}{c}\right)\right] \cdot \left\{ 1 - \operatorname{erf}\left[\frac{\sqrt{2}c\bar{x}}{4\sigma_r^2} - \frac{1}{\sqrt{2}\sigma} \left(t - \frac{2z}{c}\right)\right] \right\} \quad (72)$$

where

$$\langle N \rangle = \frac{\eta}{hf_o} \frac{\sigma_r^2}{s^2 z^2 \tan^2 \theta_T} |R(o)|^2 A_R z^{-2} T_a^2 \quad (73)$$

$$\sigma^2 = \frac{4}{c^2} \sigma_\xi^2 + \sigma_g^2 \quad (74)$$

$$\sigma_r^2 = 2z^2 (\tan^2 \theta_T + 2S^{-2})^{-1} \quad (75)$$

and $\operatorname{erf}(\cdot)$ is the error function.

In arriving at Equation (72), we have made use of the fact that $\left(1 + \frac{\rho^2}{z^2}\right)^2 = 1$ within the laser footprint. The justification behind this is that the maximum value of $\frac{\rho^2}{z^2}$ is $\tan^2 \theta_T$, and θ_T is on the order of 10^{-3} radians or smaller for a typical laser altimeter.

Equation (72) is found to be of the same form as the results obtained by Fedor et al. [3] and Hammond et al. [17] for radar altimeters.

Equation (72) is plotted in Fig. 3 through Fig. 7 for different sets of altimeter parameters and various sea states. It is observed that, for a beam divergence angle 10^{-2} radians or larger, the received waveform is

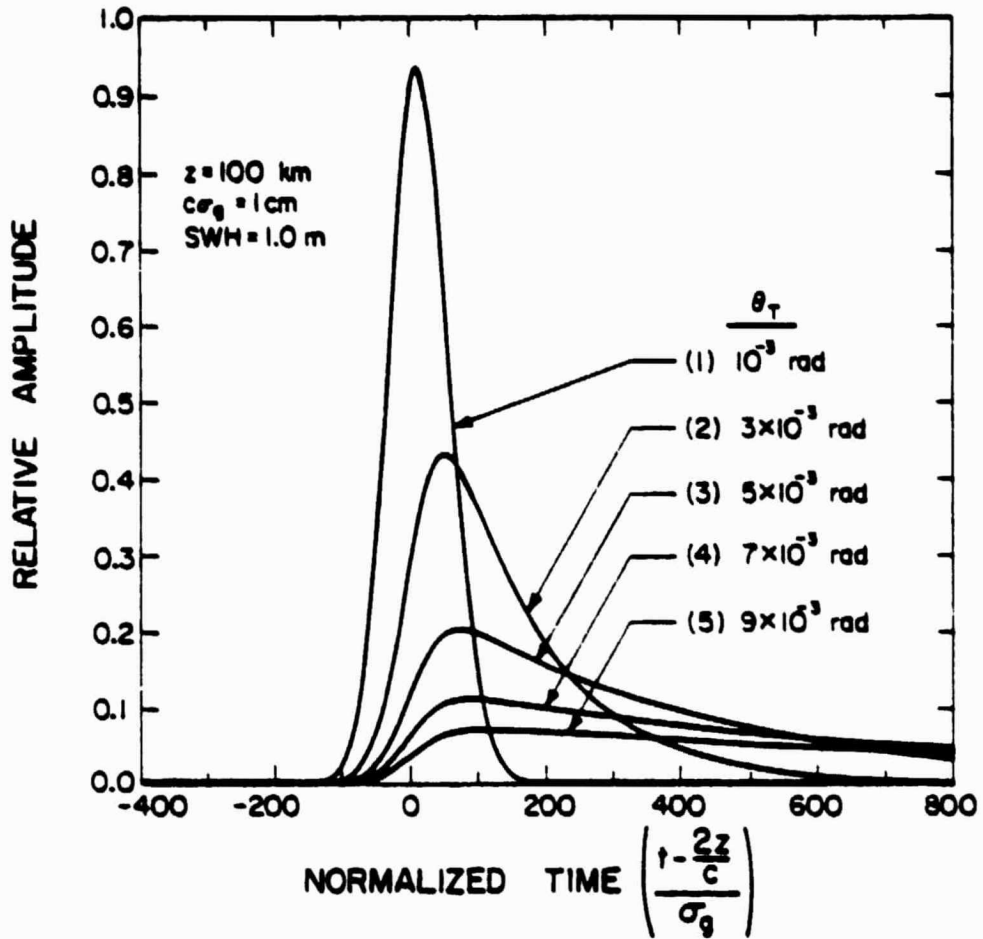


Figure 3. Mean received waveforms for laser altimeters with different beam divergence angles.

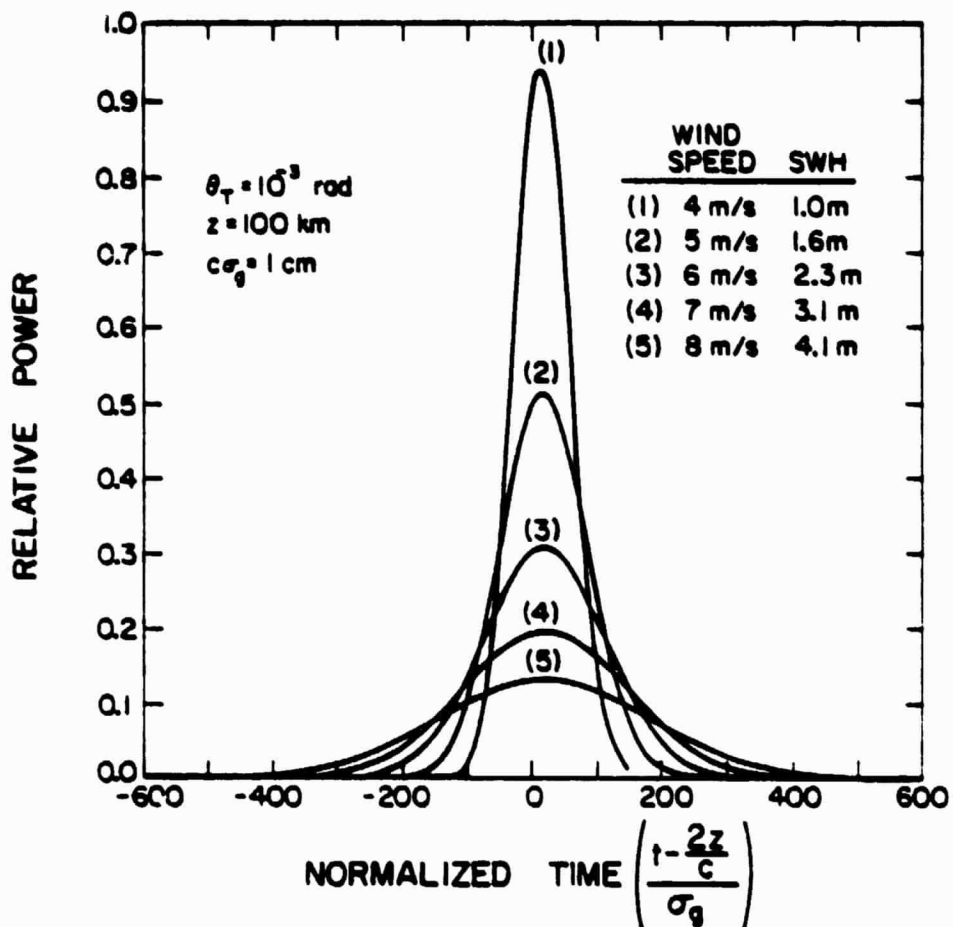


Figure 4. Mean received waveforms of the laser altimeter for different wind speed and SWH.

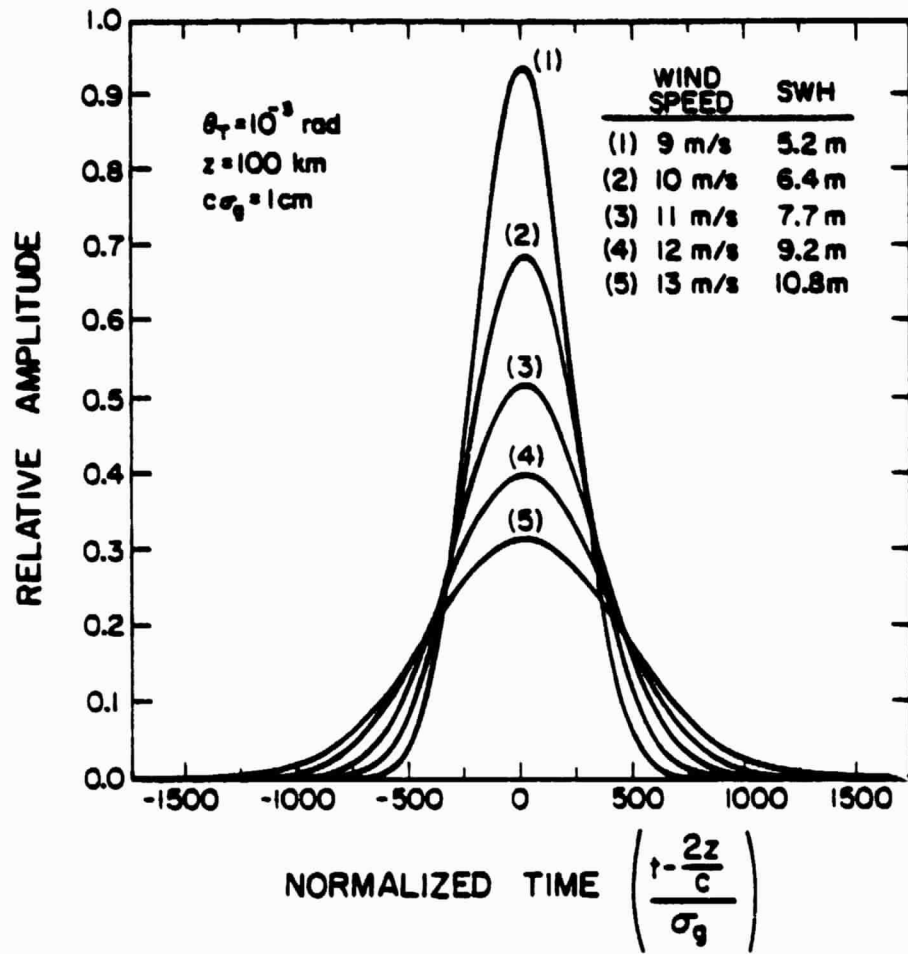


Figure 5. Mean received waveforms of the laser altimeter for different wind speed and SWH.

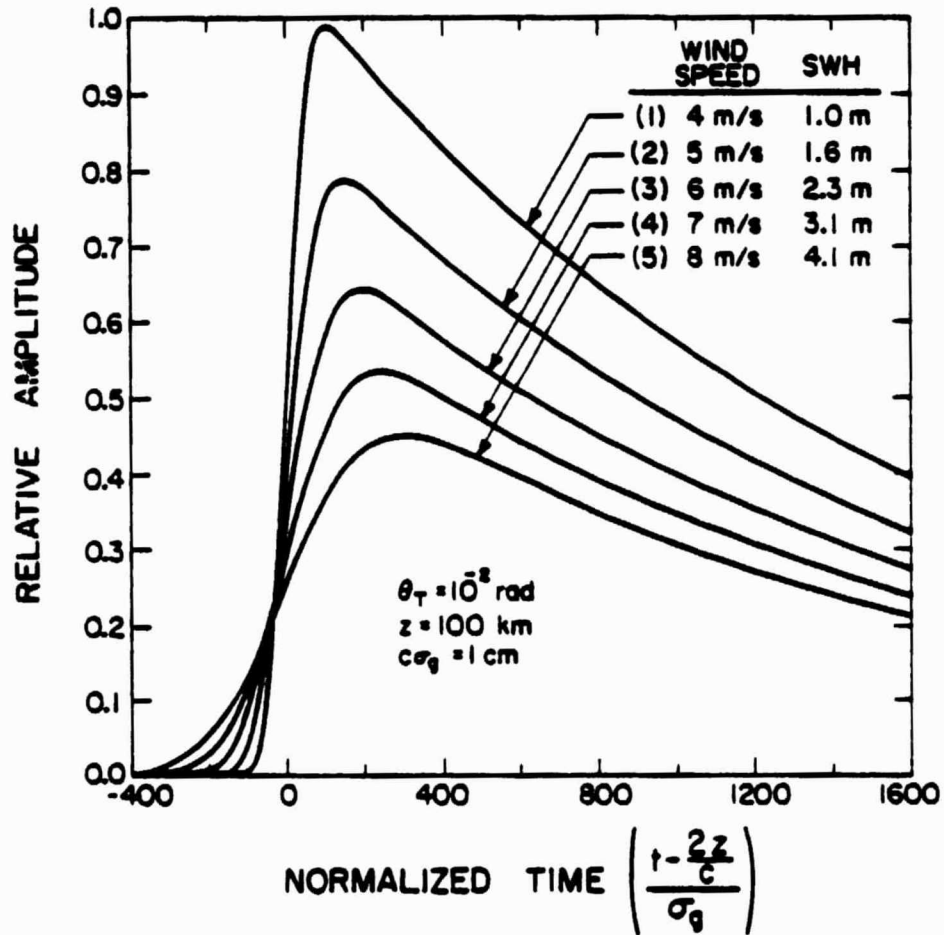


Figure 6. Mean received waveforms of the laser altimeter for different wind speed and SWH.

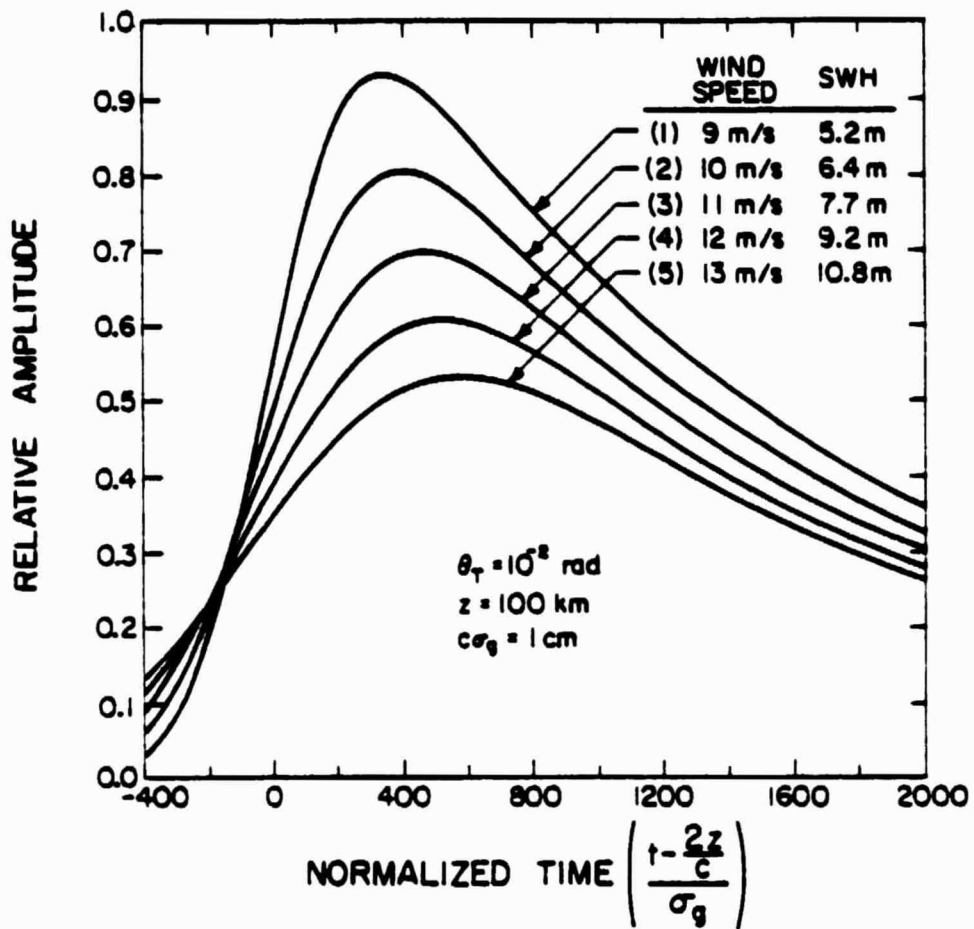


Figure 7. Mean received waveforms of the laser altimeter for different wind speed and SWH.

highly asymmetrical, and the figures obtained are similar to those obtained for radar altimeters [3], [17]. In this case, the rise time of the leading edge of the received pulse can be used to infer the roughness of the ocean surface, but the trailing edge of the received pulse is relatively insensitive to sea states [see Ref. 3].

For a beam divergence angle 10^{-3} radians or smaller, which is typical for a laser altimeter, the received waveform is found to be nearly Gaussian in shape. In this case, the centroid and rms width of the received pulse are easily identified. The expected delay, given in Equation (62), is

$$\langle T_s \rangle = \frac{2z}{c} + \frac{2z}{c} (\tan^{-2} \theta_T + 2S^{-2})^{-1} \quad (76)$$

where S is the mean square value of the total slopes, defined previously in Equation (37). Equation (76) differs from the previous result for reflections from the ground target [1] by the presence of the S^{-2} term. Ground reflections are primarily diffuse, and the reflectivity of the target is more or less uniform within the laser footprint. On the other hand, reflections from the water surface depend on the occurrence of specular points which satisfy the required slopes. From Equations (15) and (16), we see that the surface slopes required for the contributing specular points are larger for points further away from the center of the laser footprint. Since the occurrence of specular points with large surface slopes is less probable than that with small surface slopes, the effective reflectivity associated with the edge area is smaller than the reflectivity of the center area of the footprint. Therefore, upon reflection from the ocean surface, the laser cross-section is modified by the distribution of surface slopes. The S^{-2} term in Equation (76) accounts for this modification. The mean square width of the received pulse is obtained from Equation (65)

$$E[\sigma_s^2] = \sigma_h^2 + \sigma_f^2 + \frac{4}{c^2} \sigma_\xi^2 + \frac{4z^2}{c^2} (\tan^{-2} \theta_T + 2s^{-2})^{-2} \quad (77)$$

If θ_T is on the order of 10^{-3} radians or smaller, the last term in Equation (75) will be approximately equal to $\frac{4z^2}{c^2} \tan^4 \theta_T$, independent of the sea state. Therefore, an estimate of σ_ξ^2 , which is the variance of surface height can be obtained, since σ_h^2 , σ_f^2 and $\frac{4z^2}{c^2} \tan^4 \theta_T$ are all known parameters of the altimeter.

Next, we take into account the non-Gaussian nature of the ocean surface. Since we are considering normal incidence, and the divergence angle of the laser beam is very narrow, the specular points that contribute to the received field will be those facing upwards or with zero slopes. Hence, we can approximate $p(\xi_x, \xi_y, \xi)$ in Equation (23) by

$$P(\xi_x, \xi_y, \xi) \approx p(0, 0, \xi) \quad (78)$$

By using Equation (43) for $p(0, 0, \xi)$, and substituting into Equation (23) for the expected received signal, the integration can be evaluated numerically. The results are shown in Figure 8 to Figure 10 for different values of the skewness coefficient.

The mean pulse delay and mean square pulse width in this case are

$$\langle T_s \rangle = \frac{2z}{c} + \frac{2z}{c} \tan^2 \theta_T + \frac{2}{c} \lambda_3 \sigma_\xi \quad (79)$$

$$E[\sigma_s^2] = \sigma_h^2 + \sigma_f^2 + \frac{4z^2}{c^2} \tan^4 \theta_T + \frac{4}{c^2} \sigma_\xi^2 (1 - \lambda_3^2) \quad (80)$$

where λ_3 is the skewness coefficient defined previously in Equation (42). Jackson [16] pointed out that the value of λ_3 depends on the wave age and the dominant wave length. Developing seas have a greater skewness value, while old seas and swell exhibit smaller-than-equilibrium skewness values. The equilibrium value of λ_3 is about 0.2.

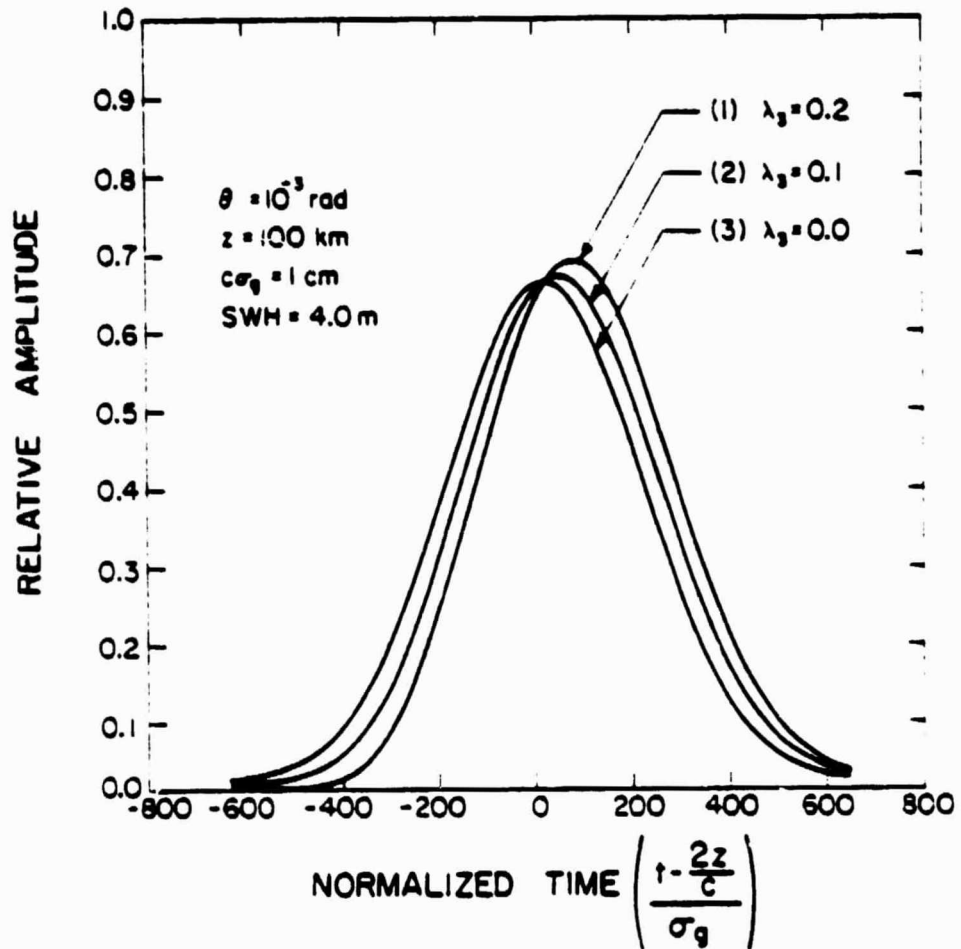


Figure 8. Mean received waveform of the laser altimeter for different values of the skewness coefficient.

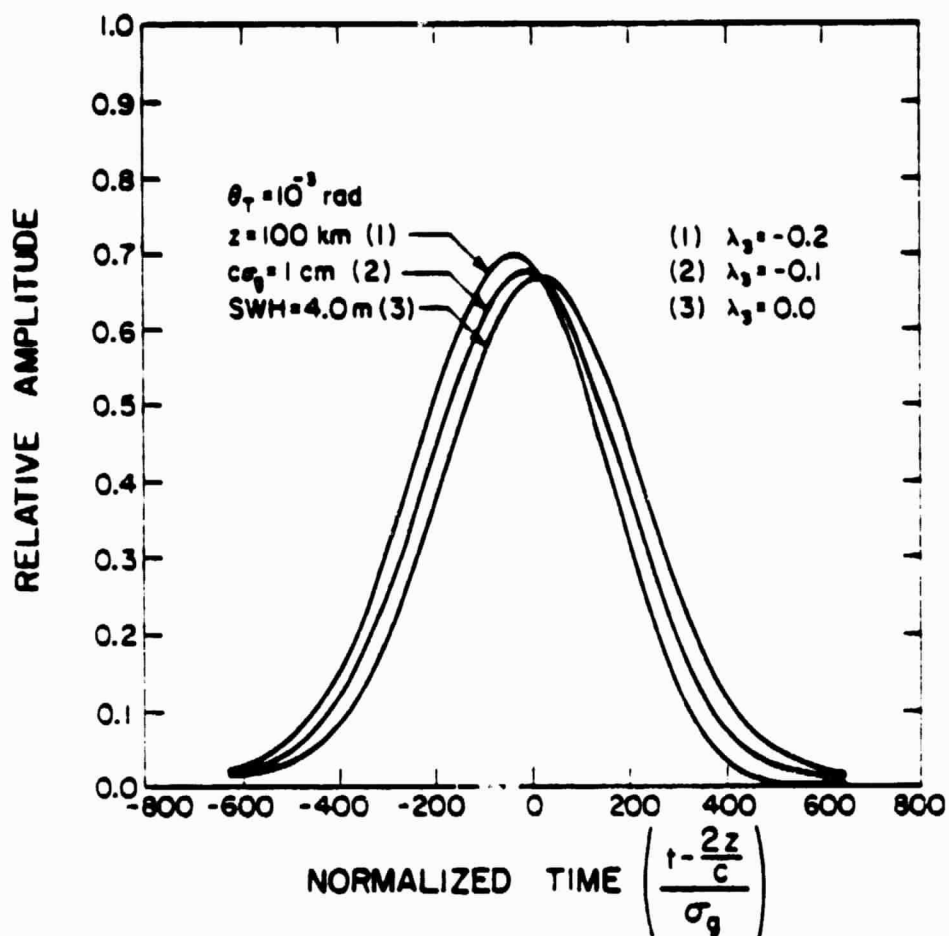


Figure 9. Mean received waveforms of the laser altimeter for different values of the skewness coefficient.

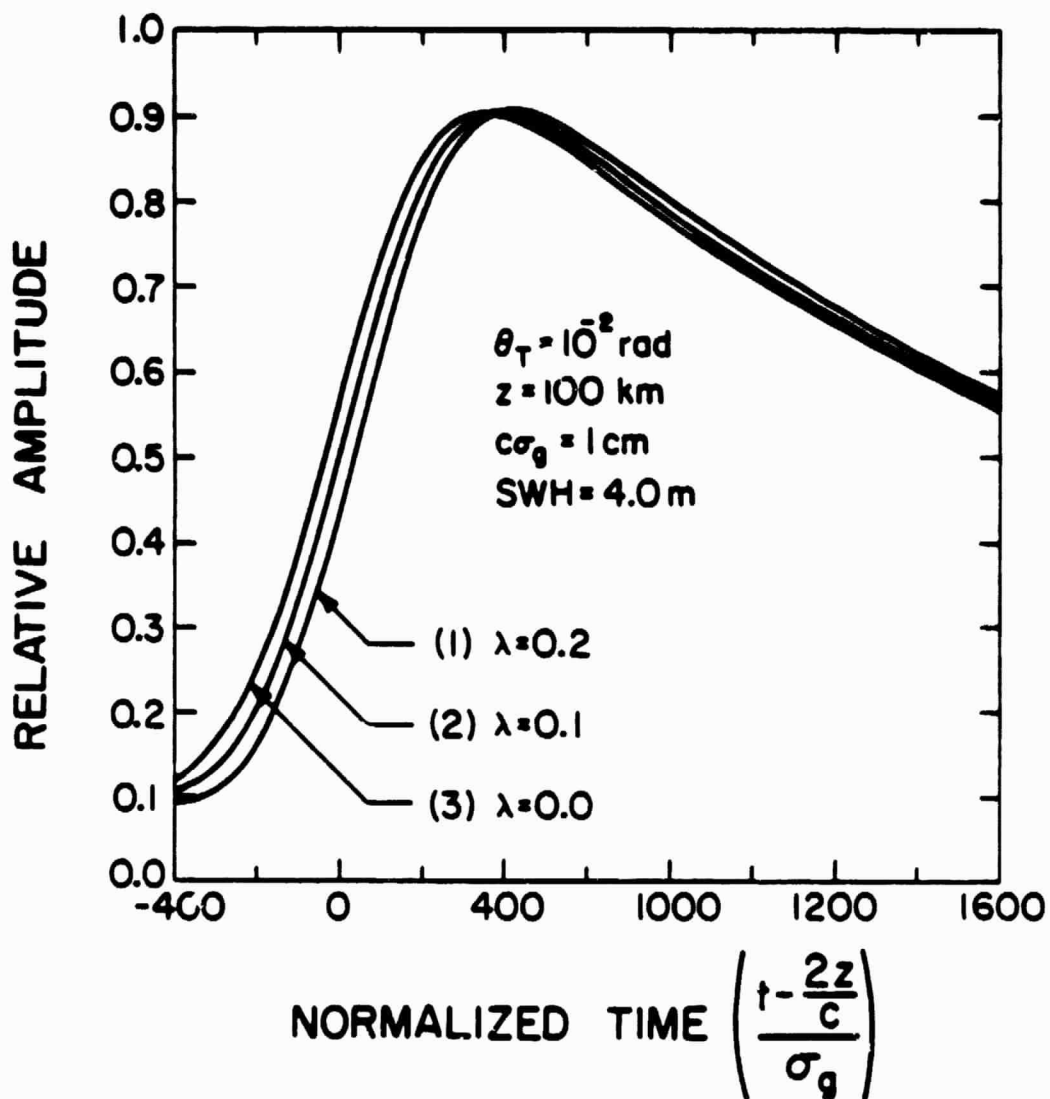


Figure 10. Mean received waveforms of the laser altimeter for different values of the skewness coefficient.

Comparing Equation (79) with Equation (76), we find there is bias in the mean of the altimeter output. In terms of altitude, the amount of bias is $\lambda_3 \sigma_\xi$, which is about 20% of the rms wave height, a significant amount considering the accuracy of the laser altimeter.

By comparing Equation (80) with (77) for the mean square pulse width, the difference is found to be about 4% of the mean square roughness σ_ξ^2 . We conclude the actual value of λ_3 is important in estimating the altitude, but is less critical if only the sea surface roughness is to be extracted from the received pulse width.

6. NON-NORMAL INCIDENCE

For the analysis in the previous sections, the laser altimeter was assumed to be pointed at nadir. If the nadir angle is small so that the shadowing effects can be neglected, the results of the previous section can be easily modified to include the effects of the nadir angle. The system geometry is illustrated in Figure 11. The expressions for the means and variances of the received pulse delay and width involve 2-D integrations over the $\underline{\rho} = (x,y)$ coordinates, which are transverse to the direction of propagation. For the geometry in Figure 11, we have chosen the nadir angle so that the propagation axis is normal to the y-axis and intersects the x-axis at the angle $\pi/2 - \phi$. In order to apply the results of the previous section, we need to determine the apparent altitude z' and apparent surface profile ξ' for the nadir pointing angle in terms of the actual altitude z and profile ξ . From simple geometrical considerations, we have

$$z' = \frac{z}{\cos \phi} \quad (81)$$

$$\xi'(\rho) = x \tan \phi + \frac{\xi(\underline{\rho}')}{\cos \phi} \quad (82)$$

$$x' = \frac{x}{\cos \phi} + \xi(\underline{\rho}') \tan \phi \quad (83)$$

$$y' = y \quad (84)$$

Again, the divergence angle of the laser beam is small, so that the following equation holds for the contributing specular points

$$p(\xi_x, \xi_y, \xi) \approx p(\tan \phi, 0, \xi) \quad (85)$$

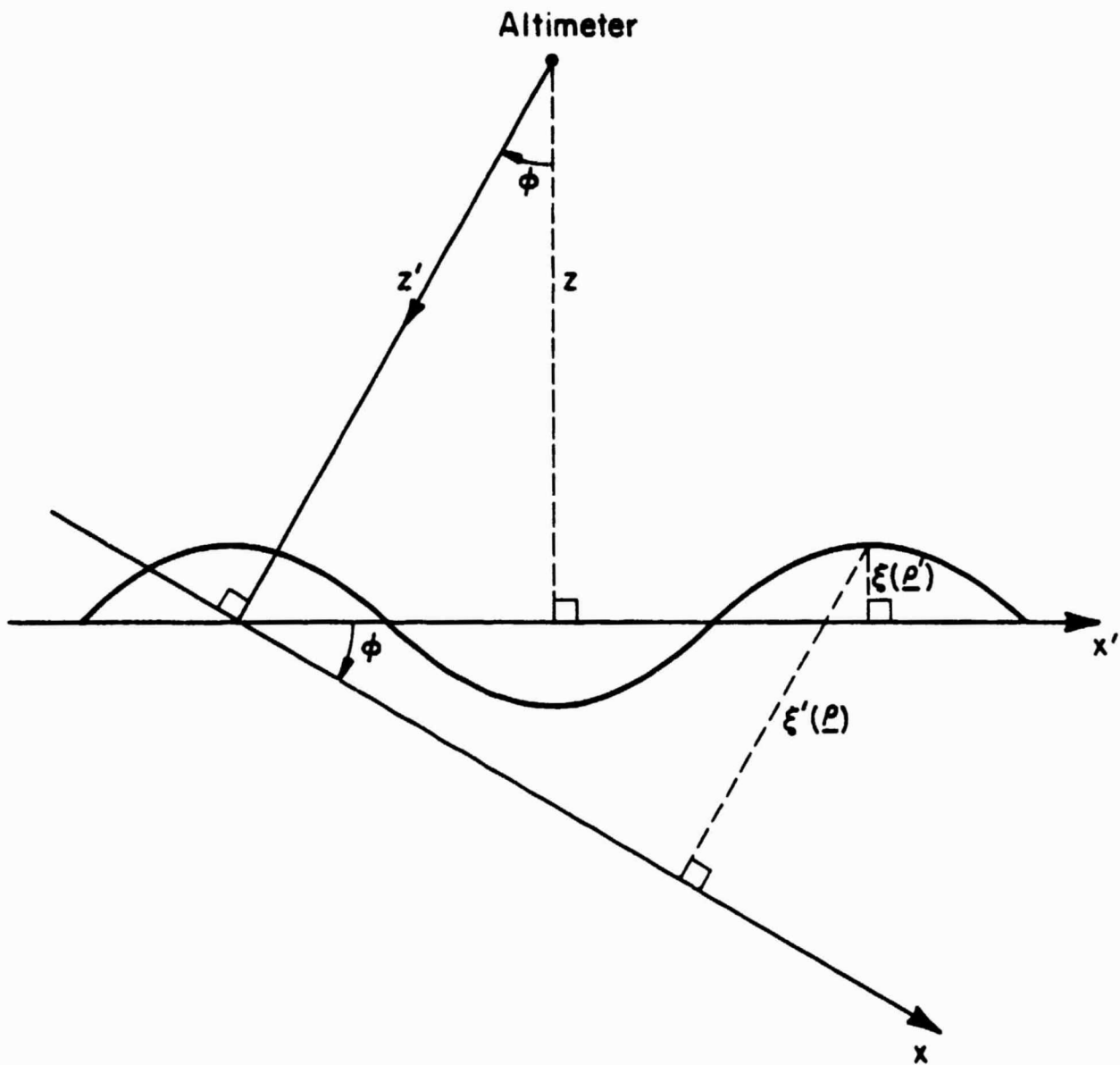


Figure 11. Geometry of the laser altimeter and ocean surface for non-normal incidence.

By modifying Equation (41) into the joint density function of surface slopes and elevation evaluated at $\xi_x = \tan \phi$, $\xi_y = 0$, we have

$$P(\tan \phi, 0, \xi) = [(2\pi^3)^{1/2} S^2 \sigma_\xi^2]^{-1/2} \exp \left[-\frac{1}{2} \left(\frac{\xi^2}{\sigma_\xi^2} + \frac{2 \tan^2 \phi}{S^2} \right) \right] \\ \cdot \left[1 + \frac{\lambda_3}{6} \left(\frac{\xi^3}{\sigma_\xi^3} - 9 \frac{\xi}{\sigma_\xi} + 6 \frac{\xi}{\sigma_\xi} \frac{2 \tan^2 \phi}{S^2} \right) \right] \quad (86)$$

In Equation (86), we have assumed that $\langle \xi_x^2 \rangle = \langle \xi_y^2 \rangle = \frac{S^2}{2}$. Using Equations (66), (70) and (86), the expected delay and mean square width of the received pulse are calculated

$$\langle T_s \rangle = \frac{2z}{c \cos \phi} + \frac{2z}{c \cos \phi} \tan^2 \theta_T + \frac{2}{c \cos \phi} \sigma_\xi \lambda_3 \left(1 - \frac{2 \tan^2 \phi}{S^2} \right) \quad (87)$$

$$E[\sigma_s^2] = \sigma_h^2 + \sigma_f^2 + \frac{4z^2}{c^2 \cos^2 \phi} \tan^4 \theta_T \\ + \frac{4\sigma_\xi^2}{c^2 \cos^2 \phi} \left[1 - \lambda_3^2 \left(1 - \frac{2 \tan^2 \phi}{S^2} \right)^2 \right] + \frac{4z^2}{c^2 \cos^2 \phi} \tan^2 \theta_T \tan^2 \phi \quad (88)$$

From Equation (87), we find that the non-zero nadir angle has increased the mean delay time by the factor $(\cos \phi)^{-1}$. For the mean square pulse width in Equation (88), the last term is the extra spreading due to the tilt of the altimeter. The origin of this term could be seen from Equation (82), where the tilt introduces a linear term into the effective profile.

The pulse spreading due to non-normal incidence will be significant if the magnitude of $z \tan \theta_T \tan \phi$ is comparable to the rms wave height σ_ξ ,

because ambiguity will then arise in determining σ_{ξ} from the received pulse width. It appears that the effect of the non-zero nadir angle can be minimized by decreasing the beam divergence angle θ_T ; however, as pointed out by Gardner [1], this is achieved at the cost of higher speckle induced noise.

7. CONCLUSIONS

In previous chapters, we have shown that a short pulse laser altimeter can be used in the determination of mean sea level and sea states. Since a much narrower pulse width can be transmitted by a laser altimeter than by a radar altimeter, the inherent resolution of the laser altimeter is clearly higher. We point out that to fully achieve the high accuracy promised by a laser altimeter further research on the statistical properties of capillary waves and their interactions with optical radiation has to be done. Also, on the true sea surface, whitecaps and foam patches begin to form as wind speed increases. Foam patches and whitecaps contain sprays and bubbles that cause scattering which is not easy to analyze theoretically; their effects on the received signal may or may not be significant, and should be determined by future experimental work.

Results of Chapter 6 indicate that nadir angle effects enter the estimates of both the mean sea level and SWH. When the altimeter is at orbital altitudes, it is necessary to measure the nadir angle to a high degree of accuracy, since an error on the order of milliradians can cause erroneous estimates of the mean sea level and SWH.

REFERENCES

- [1] C. S. Gardner, "Analysis of target signature for laser altimeters," RRL Publication No. 510, Radio Res. Lab., Dep. Elec. Eng., Univ. of Ill. Urbana-Champaign.
- [2] W. F. Townsend, "An initial assessment of the performance achieved by the Seasat-1 radar altimeter," IEEE J. Oceanic Eng., vol. OE-5, no. 2, pp. 80-92, April 1980.
- [3] L. S. Fedor, T. W. Godbey, J. F. R. Gower, R. Guptill, G. S. Hayne, C. L. Rufenach and E. J. Walsh, "Satellite altimeter measurements of sea state - An algorithm comparison," J. Geophys. Res., vol. 84, no. B8, pp. 3991-4001, July 1979.
- [4] R. D. Kodis, "A note on the theory of scattering from an irregular surface," IEEE Trans. Antennas Propagat., vol. AP-14, no. 1, pp. 77-82, January 1966.
- [5] M. I. Skolnik, "Introduction to radar system." New York: McGraw-Hill, p. 34, 1980.
- [6] D. E. Barrick, "Rough surface scattering based on the specular point theory," IEEE Trans. Antennas Propagat., vol. AP-16, no. 4, pp. 449-454, July 1968.
- [7] A. Papoulis, "Estimation of the average density of a nonuniform Poisson process," IEEE Trans. Comm., vol. COM-22, no. 2, pp. 162-167, February 1974.
- [8] J. W. Goodman, "Statistical properties of laser speckle patterns," in Laser Speckle and Related Phenomena, J. C. Dainty, Ed. New York: Springer-Verlag, pp. 9-65, 1975.
- [9] C. S. Gardner, "Correction of laser tracking data for the effects of horizontal refractivity gradients," Appl. Opt., vol. 16, no. 9, pp. 2427-2432, September 1977.
- [10] O. M. Phillips, The Dynamics of the Upper Ocean. London: Cambridge University Press, Chapter 4, 1977.
- [11] D. E. Barrick, "Remote sensing of sea state by radar," in Remote Sensing of the Troposphere, V. E. Derr, Ed., U. S. Government Printing Office, Chapter 12, 1972.
- [12] M. S. Longuet-Higgins, "The effect of non-linearities on statistical distributions in the theory of sea waves," J. Fluid Mech., vol. 17, part 3, pp. 459-480, 1963.
- [13] C. Cox and W. Munk, "Measurement of the roughness of the sea surface from photographs of the sun's glitter," J. Opt. Soc. Amer., vol. 44, no. 11, pp. 838-850, November 1954.

- [14] B. S. Yaplee, A. Shapiro, D. L. Hammond, B. D. Au and E. A. Uliana, "Nanosecond radar observations of the ocean surface from a stable platform," IEEE Trans. Geosci. Electron., vol. GE-9, no. 3, pp. 170-174, July 1971.
- [15] J. Buffton, private communication.
- [16] F. C. Jackson, "The reflection of impulses from a nonlinear random sea," J. Geophys. Res., vol. 84, pp. 4939-4943, August 1979.
- [17] D. L. Hammond, R. A. Mennella and E. J. Walsh, "Short pulse radar used to measure sea surface wind speed and SWH," IEEE Trans. Antennas Propagat., vol. AP-25, no. 1, pp. 61-66, January 1977.

CUMULATIVE LIST OF RADIO RESEARCH LABORATORY REPORTS

PREPARED UNDER NASA GRANT NSG-5049

- RRL Rep. No. 469 - Gardner, C. S. (December 1975), The Effects of Random Path Fluctuations on the Accuracy of Laser Ranging Systems.
- RRL Rep. No. 471 - Zanter, D. L., C. S. Gardner and N. N. Rao (January 1976), The Effects of Atmospheric Refraction on the Accuracy of Laser Ranging Systems.
- RRL Rep. No. 477 - Gardner, C. S. and J. R. Rowlett (November 1976), Atmospheric Refraction Errors in Laser Ranging Data.
- RRL Rep. No. 478 - Gardner, C. S. and B. E. Hendrickson (December 1976), Correction of Laser Ranging Data for the Effects of Horizontal Refractivity Gradients.
- RRL Rep. No. 481 - Gardner, C. S. (January 1977), Statistics of the Residual Refraction Errors in Laser Ranging Data.
- RRL Rep. No. 486 - Gardner, C. S. (June 1977), Comparison Between the Refraction Error Covariance Model and Ray Tracing.
- RRL Rep. No. 488 - Gardner, C. S. (December 1977), Speckle Noise in Satellite Based Lidar Systems.
- RRL Rep. No. 495 - Gardner, C. S. and G. S. Mecnerle (April 1978), Speckle Noise in Direct-Detection Lidar Systems.
- RRL Rep. No. 496 - Gardner, C. S. and A. M. Saleh (October 1978), Speckle Noise in Differential Absorption Lidar Systems.
- RRL Rep. No. 499 - Gardner, C. S. (January 1979), A Technique for Remotely Measuring Surface Pressure from a Satellite Using a Multicolor Laser Ranging System.

RRL Rep. No. 502 - Palluch, E., J. Shelton and C. S. Gardner (May 1979),
Operating Manual for the RRL 8 Channel Data Logger.

RRL Rep. No. 505 - Gardner, C. S. and R. Axford, Jr. (March 1980),
Regression Models for Multicolor Satellite Laser Ranging.

RRL Rep. No. 510 - Gardner, C. S. (April 1981), Analysis of Target
Signatures for Laser Altimeters.

RRL Rep. No. 514 - Tsai, B. and C. S. Gardner (December 1981), Remote
Sensing of Sea State by Laser Altimeters.

PAPERS PUBLISHED

- C. S. Gardner, "Effects of Random Path Fluctuations on the Accuracy of Laser Ranging Data," Applied Optics, 15, 2539-2545, October 1976.
- C. S. Gardner, "Effects of Horizontal Refractivity Gradients on the Accuracy of Laser Ranging to Satellites," Radio Science, 11, 1037-1044, December 1976.
- C. S. Gardner, "Correction of Laser Tracking Data for the Effects of Horizontal Refractivity Gradients," Applied Optics, 16, 2427-2432, September 1977.
- C. S. Gardner, J. R. Rowlett, and B. E. Hendrickson, "Ray Tracing Evaluation of a Technique for Correcting the Refraction Errors in Satellite Tracking Data," Applied Optics, 17, 3143-3145, October 1978.
- C. S. Gardner, "Technique for Remotely Measuring Surface Pressure from a Satellite using a Multicolor Laser Ranging System," Applied Optics, 18, 3184-3189, September 15, 1979.
- C. S. Gardner, "Target Signatures for Laser Altimeters: An Analysis," Applied Optics, 21, January 15, 1981.